High probability of triggering climate tipping points under current policies modestly amplified by Amazon dieback and permafrost thaw

Jakob Deutloff[1, 2, 3], Hermann Held[4], and Timothy M Lenton[1]

[1]Global Systems Institute, University of Exeter, Exeter, UK.
[2]Center for Earth System Research and Sustainability (CEN), Meteorological Institute, Universität Hamburg, Hamburg, Germany.
[3]International Max Planck Research School on Earth System Modelling (IMPRS-ESM), Hamburg, Germany.
[4]Research Unit Sustainability and Global Change and Center for Earth System Research and Sustainability, Universität Hamburg, Germany.

Correspondence: Jakob Deutloff (jakob.deutloff@mpimet.mpg.de)

Abstract. We investigate the probabilities of triggering climate tipping points under various shared socioeconomic pathways (SSPs), and how they are altered by including the additional carbon emissions that could arise from tipping points within the Earth's carbon cycle. Crossing of a climate tipping point at a threshold level of global mean surface temperature (threshold temperature), would commit the affected subsystem of the Earth to abrupt and largely irreversible changes with negative impacts on human well-being. However, it remains unclear which tipping points would be triggered under the different SSPs, due to uncertainties in the climate sensitivity to anthropogenic greenhouse gas emissions, the threshold temperatures of climate tipping points, and the response of tipping points within the Earth's carbon cycle to global warming. We include those uncertainties in our analysis to derive probabilities of triggering for 16 previously-identified climate tipping points within the Earth system. To conduct our analysis, we use the reduced complexity climate model FaIR which is coupled to a conceptual model of the tipping processes within the Amazon rainforest and permafrost, which are the two major tipping elements within the Earth's carbon cycle. Uncertainties are propagated by employing a Monte Carlo approach for the construction of large model ensembles. We find that SSP2-4.5, which compares best to the warming trajectory expected from current policies, is highly unsafe with regard to triggering climate tipping points. Averaged over all 16 tipping points, the probability of triggering until the year 2500 is 64% under SSP2-4.5, and eight tipping points have a more than 66% probability of getting triggered. The additional warming from abrupt Amazon dieback and permafrost thaw increases the risk for high temperature pathways, but on average remains small compared to the anthropogenic warming. Under SSP2-4.5, abrupt Amazon dieback and permafrost thaw add 0.15°C $(0.03 - 0.91$°C$)$ to global warming in 2500. This additional warming increases the average probability of triggering until 2500 by 3.3 percent points under SSP2-4.5. Even though this is the maximum triggering probability increase caused by carbon emissions from the Amazon and permafrost among all SSPs, it still remains modest compared to the probability of triggering caused by anthropogenic warming. The risk of triggering climate tipping points is reduced significantly under SSP1-2.6 with average probabilities of triggering until 2500 of 37%, which is increased by 2.2 percent points due to carbon emissions from the Amazon and permafrost.

1 Introduction

The term "tipping point" is commonly used to describe a critical threshold in the forcing of a system, at which small additional forcing leads to significant and long-term changes of the system (Lenton et al., 2008). The debate about tipping points in the climate system, referred to as "climate tipping points", has intensified over the past two decades. Increasing numbers of Earth system components have been identified which could possibly exhibit tipping behaviour (e.g. Lenton et al., 2008; Kriegler et al., 2009; Steffen et al., 2018), with 15 candidates being shortlisted in the latest IPCC report (Lee et al., 2021). These Earth system components are referred to as "tipping elements" (TEs) and occur within the biosphere, cryosphere and oceanic or atmospheric circulation (Lenton et al., 2008). The global mean surface temperature (GMST) relative to pre-industrial levels is used as a common metric to describe the forcing of the TEs (Armstrong McKay et al., 2022). This means that a tipping point can be associated with a "threshold temperature" after which the respective TE is expected to exhibit tipping behaviour. There is growing concern about the possible proximity of climate tipping points, as threshold temperatures have been revised to lower levels, with some TEs being at risk of getting "triggered" (crossing of their threshold temperature) at GMST values as low as $1°C$ (Lenton et al., 2019).

In their recent literature synthesis, Armstrong McKay et al. (2022) identify 16 TEs within the Earth system and provide estimates of their threshold temperatures, the characteristic timescales their tipping is assumed to unfold over, and their impact on global warming (Table 1, we will use the abbreviations defined in the table for the different TEs). Building on the definition of TEs by Lenton et al. (2008), Armstrong McKay et al. (2022) distinguish between "global core" and "regional impact" TEs. To qualify as a global core TE, a tipping point has to occur uniformly across a sub-continental scale ($\sim 1000\,\text{km}$) for a subsystem of the Earth. However, if the change in forcing is approximately uniform across a large spatial area, small-scale tipping points can be crossed near-synchronously at a sub-continental scale, which qualifies the affected subsystem as a regional impact TE. Furthermore, global TEs have to contribute significantly to the overall operation mode of the Earth system, while regional impact TEs are required to either contribute significantly to human welfare or to have great value in themselves as unique features of the Earth system.

Since triggering of TEs will negatively affect human welfare, political efforts should be increased to avoid them (Cai et al., 2016). However, it is not straightforward to determine how safe a specific emission scenario is with regard to triggering TEs, since several uncertainties need to be accounted for within this calculation. The climate sensitivity to anthropogenic emissions remains poorly constrained, with a likely range of the equilibrium climate sensitivity to a doubling of atmospheric CO_2 concentrations of $2.5 - 4°C$ (Chen et al., 2021). Furthermore, climate tipping points include uncertainties within their threshold temperatures, timescales, impacts and for some even their existence remains uncertain (Armstrong McKay et al., 2022). Additional uncertainty is introduced by potential interactions of climate tipping points, which tend to destabilize them (Wunderling et al., 2021). Such interactions can be of manifold nature and often involve complex mechanisms. One example are TEs within the Earth's carbon cycle, which have the potential to release large amounts of greenhouse gases (GHGs) and thereby amplify global warming, which in turn increases the probability of triggering other TEs (Steffen et al., 2018).

In this study, we calculate probabilities of triggering for the 16 TEs that Armstrong McKay et al. (2022) identify within the Earth system, including the uncertainties in climate sensitivities and the threshold temperatures, by employing a Monte Carlo approach (Metropolis et al., 1953). Herewith, we provide an update of the widely used but somewhat outdated probabilities of triggering derived from an expert elicitation conducted by Kriegler et al. (2009). Furthermore, we quantify the additional warming that might arise from TEs within the Earth's carbon cycle and how it increases the probabilities of triggering other TEs.

TEs with the potential to significantly impact the Earth's carbon cycle include abrupt permafrost thaw or collapse, Amazon rainforest dieback and northern expansion and southern dieback of boreal forest (Armstrong McKay et al., 2022). Since northern expansion and southern dieback of boreal forests balance out in terms of global warming, we exclude them from our analysis. The exact nature of this balance remains contested. The latest IPCC report assumes that expansion of boreal forest at their northern edge and dieback of boreal forest accompanied by temperate forest invasion at the southern edge of boreal forests will roughly balance out in terms of carbon emissions (Canadell et al., 2021). On the other hand, Armstrong McKay et al. (2022) argue that the carbon release from southern dieback will be an order of magnitude larger than the sequestered carbon from northern expansion of boreal forests, but the warming would still balance out since it is to first order determined by albedo and evapotranspiration changes (Table 1).

Permafrost thaw can be further subdivided into three distinct processes: gradual permafrost thaw, which is a threshold-free feedback to global warming; abrupt permafrost thaw, which is a regional impact tipping element; permafrost collapse, which is a global core tipping element (Armstrong McKay et al., 2022). Since gradual thaw of permafrost, associated with uniform and large-scale deepening of the active layer, is not assumed to include a tipping point, we do not include it in our analysis. Instead, we focus on abrupt thaw and collapse of permafrost and Amazon dieback, hereafter referred to as the "carbon tipping elements".

Abrupt thaw of permafrost occurs regionally but near-synchronously over the permafrost region due to thermokarsts which can affect several meters of permafrost within days to weeks (Turetsky et al., 2019). The emerging landscapes mostly include water-saturated soils (Olefeldt et al., 2016), hence high methane emissions from anaerobic respiration of the now accessible soil organic carbon must be expected. Around 20% of the carbon emissions from abrupt permafrost thaw are assumed to be released as methane (Turetsky et al., 2020). Abrupt permafrost thaw is assumed to amplify gradual thaw, since they spread at similar rates in dedicated permafrost models (Turetsky et al., 2020; Armstrong McKay et al., 2022).

Collapse of permafrost can be caused by permafrost degradation becoming self-perpetuating due to the heat released by microbial respiration of soil organic carbon, leading to further thaw of permafrost and resulting in a positive feedback loop, which is referred to as the "compost bomb instability" (Luke and Cox, 2011; Khvorostyanov et al., 2008). This process might occur in the Yedoma region or in abruptly dried permafrost soils (Armstrong McKay et al., 2022).

Abrupt dieback of the Amazon is assumed to occur due to reduced moisture recycling and forest-fire-feedbacks triggered by initial tree loss due to either global warming or deforestation, whereby only the former is accounted for in this study (Science Panel for the Amazon, 2021; Nobre et al., 2016).

90 Our model framework relies on the second version of the Finite amplitude Impulse Response model (FaIR), a 0D reduced complexity climate model developed by Leach et al. (2021), and the estimates for the threshold temperatures, timescales, and impacts of TEs from Armstrong McKay et al. (2022). These estimates are used to build a conceptual carbon tipping elements model (CTEM), which can be coupled to FaIR to include the additional carbon emissions from carbon TEs. With this setup, we generate a "coupled" (CTEM coupled to FaIR) and an "uncoupled" (FaIR only) large-scale model ensemble for all Tier1 shared

95 socioeconomic pathways (SSPs) except for SSP1-1.9 (O'Neill et al., 2016). Hereby, we propagate the involved uncertainties, up until the year 2500.

  We exclude SSP1-1.9 from our analysis since it includes a temperature "overshoot" with a pronounced peak of GMST (IPCC, 2021). In case of such a temperature overshoot, tipping elements with internal timescales longer than the period for which GMST exceeds their threshold temperature might remain in their stable baseline state (Ritchie et al., 2021). However, the

100 internal timescales of tipping elements remain highly uncertain, which is why we don't consider the possibility for overshoot of threshold temperatures in this study. To assess the risk of current policies for triggering climate tipping points, we focus our analysis on SSP2-4.5. With a median warming of 2.8°C in 2100 produced by FaIR, this scenario is closest to the estimated warming in 2100 resulting from current policies (2.7°C (Climate Action Tracker, 2022), 2.8°C (United Nations Environment Programme, 2022), 2.6°C (Meinshausen et al., 2022)).

105 Our approach is explained in more detail in the next section. In section 3 we investigate the carbon emissions and in section 4 the additional warming from carbon TEs, followed by a presentation of the probabilities of triggering TEs in section 5. We discuss our results in section 6 and conclude with section 7.

2 Data and Methods

2.1 SSP Emission Pathways

110 We use the CMIP6 GHG and aerosol emissions and effective radiative forcing datasets employed in the Reduced Complexity Model Intercomparison Project (Nicholls et al., 2020). Both datasets contain global average values with an annual timestep throughout the historical period (1750-2014) which shifts to a decadal timestep for the projection period (2015-2500).

  The CMIP6 GHG and aerosol emission projections for the five different SSP scenarios follow Gidden et al. (2019). The emission extensions beyond 2100 follow the conventions described in Meinshausen et al. (2020). Historical emissions (1750–2014)

115 of chemically reactive gases (CO, CH_4, NH_3, NO_x, SO_2, non-methane volatile organic compounds) carbonaceous aerosols (black carbon and organic carbon) and CO_2 come from the Community Emissions Data System (Hoesly et al., 2018). Historical biomass burning emissions of CH_4, black carbon, CO, NH_3, NO_X, organic carbon, SO_2 and non-methane volatile organic compounds come from Van Marle et al. (2017). Global historical CO_2 emissions from land-use are taken from the Global Carbon Budget 2016 (Le Quéré et al., 2016). Regional breakdown of land-use CO_2 emissions and N_2O emissions come from

120 the Potsdam Real-time Integrated Model for probabilistic Assessment of emissions Paths for historical emissions version 1.0 (Guetschow et al., 2016). Data gaps in the historical emissions were filled with inverse emissions based on CMIP6 concentra-

Category		Proposed Climate Tipping Element (& Tipping Point)	Threshold (°C)			Timescale (years)			Max. Impact (GtC)
			Est.	Min	Max	Est.	Min	Max	
Global core tipping elements	PFTP	Boreal Permafrost (collapse)	4.0	3.0	6.0	50	10	300	125 - 250
	GrIS	Greenland Ice Sheet (collapse)	1.5	0.8	3.0	10k	1k	15k	
	WAIS	West Antarctic Ice Sheet (collapse)	1.5	1.0	3.0	2k	500	13k	
	EAIS	East Antarctic Ice Sheet (collapse)	7.5	5.0	10.0	?	10k	?	
	EASB	East Antarctic Subglacial Basin (collapse)	3.0	2.0	6.0	2k	500	10k	
	AWSI	Arctic Winter Sea Ice (collapse)	6.3	4.5	8.7	20	10	100	
	AMAZ	Amazon Rainforest (dieback)	3.5	2.0	6.0	100	50	200	Partial: 30 Total: 75
	AMOC	Atlantic M. O. Circulation (collapse)	4.0	1.4	8.0	50	15	300	
	LABC	Labrador- Irminger Seas SPG Convection (collapse)	1.8	1.1	3.8	10	5	50	
Regional impact tipping elements	PFAT	Boreal Permafrost (abrupt thaw)	1.5	1.0	2.3	200	100	300	Adds 25-75% to gradual thaw: = 5-15 GtC per °C @2100; 12.5-37.5 GtC per °C @2300, up to max. 60-195 GtC
	BARI	Barents Sea Ice (abrupt loss)	1.6	1.5	1.7	25	?	?	
	GLCR	Mountain Glaciers (loss)	2.0	1.5	3.0	200	50	1k	
	REEF	Low-latitude Coral Reefs (die-off)	1.5	1.0	2.0	10	-	-	
	SAHL	Sahel and W. African Monsoon (greening)	2.8	2.0	3.5	50	10	500	
	BORF	Boreal Forest (southern dieback)	4.0	1.4	5.0	100	50	?	52 GtC / -0.18°C
	TUND	Boreal Forest (northern expansion)	4.0	1.5	7.2	100	40	?	-6 GtC / +0.14°C
Threshold-free nonlinear Feedbacks	PFGT	Boreal Permafrost (gradual thaw)	1.5	1.0	2.4	300	100	300<	20 GtC per °C @2100; 50 GtC per °C @2300, up to max 260 GtC

Table 1. Category, threshold, timescale, and impact of the TEs, reproduced from Armstrong McKay et al. (2022). Colours of the second left column represent the Earth system domain of the tipping point (blue = cryosphere, green = biosphere, orange = ocean/atmosphere). All other colours represent confidence, with green = high confidence, yellow = medium confidence and red = low confidence.

tions from the Model for the Assessment of Greenhouse Gas Induced Climate Change (MAGICC) 7.0.0 (Meinshausen et al., 2020).

Effective radiative forcing for CMIP6 follows the data provided by Smith (2020).

 ## 2.2 The FaIR Model

To map GHG and aerosol emissions to GMST, including the uncertainty in ECS, we use the FaIR v2.0.0 model developed by Leach et al. (2021), which is run with an annual timestep. It consists of six equations, five of which are adopted from Myhre et al. (2013). The sixth equation implements a state-dependency of the carbon cycle, which enables a better representation of the relationship between emissions and atmospheric concentrations for historical observations and projections (Leach et al., 2021). Despite its relative simplicity, FaIR is flexible enough to emulate more complex ESMs from CMIP6. FaIR allows for probabilistic projections of GMST by relying on a parameter ensemble informed by CMIP6 models and constrained with the observed trend and level of global warming. However, this constraint is not strong enough to rule out potentially unrealistic high equilibrium climate sensitivities (ECS) with a 95th percentile of 6.59°C, compared to 5°C reported by Forster et al. (2021). Since we rely on this constrained parameter ensemble to include the uncertainty in ECS in our predictions of GMST, extremely high temperatures towards the end of the model period might be unrealistic.

2.3 Carbon Tipping Elements Model

We introduce the simple, system-dynamics type model CTEM to investigate the carbon emissions that might arise from tipping of AMAZ, PFTP and PFAT and the respective warming caused by them, which, in turn, increases the probabilities of triggering other TEs. CTEM is able to represent the carbon emissions from AMAZ, PFAT, and PFTP, with threshold temperatures, timescales, and impacts consistent with the estimates from Armstrong McKay et al. (2022) (Table 1). Each TE is represented by a stock of cumulative carbon emissions it adds to the SSP carbon emissions. The cumulative emissions are represented by the following logistic equation:

$$\frac{dS}{dt} = r\left(\frac{T}{P}\right) S \left(1 - \frac{S}{K}\right),$$ (1)

with S being cumulative carbon emissions (in GtC), r the maximum growth rate (in yr^{-1}), K the maximum impact (in GtC), P the threshold temperature (in °C), T GMST relative to pre-industrial levels (in °C) and t time (in years). The rate-dependence of all three TEs found by Armstrong McKay et al. (2022) is included by the term T/P, which means higher exceedance of the threshold temperature causes faster change in S.

For AMAZ and PFTP, the impact is independent of GMST once they are triggered (Table 1). Therefore, Eq. 1 can be used to represent them without further modifications being necessary. PFAT, however, is assumed to amplify PFGT, which is a threshold-free feedback. Therefore, the impact of PFAT also depends on GMST, with higher temperatures leading to increased carbon emissions, and different values for this feedback in 2100 and 2300 (Table 1). Hence, for PFAT K from Eq. 1 needs to be calculated as

$$K = \min(F \cdot T, \, K_{\max})$$ (2)

with

$$F = \begin{cases} F_{100} & \forall\, t \leq 2100 \\ F_{100} \cdot \frac{2300-t}{200} + F_{300} \cdot \frac{t-2100}{200} & \forall\, 2100 < t < 2300 \\ F_{300} & \forall\, t \geq 2300 \end{cases} \tag{3}$$

Here, K is calculated as the product of the feedback strength F (in GtC °C^{-1}) and GMST (in °C), limited to the maximum impact $K_{\max}$ (in GtC) of PFAT. In Eq. 3, we define F as the feedback strength for the year 2100 (F_{100}) before and in 2100, as the feedback strength for the year 2300 (F_{300}) in and after 2300 and interpolate linearly between these two values between 2100 and 2300.

The resulting set of three differential equations (one for each TE) is solved using a forward difference scheme, similar to the implementation of FaIR (supplement of Leach et al. (2021)). In FaIR, output variables such as T are assumed to be average values between two consecutive timesteps (denoted by a bar over t), while the values for the input variables such as the annual SSP GHG emissions (E_{SSP}) reside at each timestep (no bar over t). To be consistent with this implementation, we define S and the resulting annual carbon emissions from each TE (E_{TE}) also at each timestep (Fig. S1). To calculate S for each timestep (t) with a step size (Δt) of one year, we integrate Eq. 1 which yields:

$$S(t) = \left(e^{-a(\overline{t-1})\Delta t} \left(S^{-1}(t-1) - \frac{b(\overline{t-1})}{a(\overline{t-1})} \right) + \frac{b(\overline{t-1})}{a(\overline{t-1})} \right)^{-1}, \tag{4}$$

with the auxiliary variables a and b being calculated as

$$a(\overline{t-1}) = r\frac{T(\overline{t-1})}{P}$$
$$b(\overline{t-1}) = \frac{rT(\overline{t-1})}{PK}.$$

For PFTP and AMAZ Eq. 4 can be used directly to calculate S, but for PFAT K needs to be calculated using Eq. 2 with $T = T(\overline{t-1})$ and is therefore also time-dependent (for the full derivation please see Section S2). Irreversibility of carbon emissions from all three TEs is implemented by setting negative changes of S to zero.

CTEM needs to be calibrated to match the estimated behaviour summarised in Table 1. While values for F_{100}, F_{300}, K, $K_{\max}$, and P can be used in CTEM directly, r and the initial stock (S_0) need to be calibrated or defined for the model to match the proposed tipping timescales (H). For this purpose, we define the H as the period over which 99% of the cumulative emissions occur. While H and the corresponding value of r are calibrated for the whole range of H given in Table 1 for PFTP and AMAZ, PFAT is implemented slightly different since K depends on T (Eq. 2). For PFAT, H is included implicitly in the feedback parameters F_{100} and F_{300}, with high values corresponding to short H and vice versa. Therefore, we keep H and the corresponding r fixed at their mean value for PFAT, with varying values for the feedback parameters. In the calibrated version of CTEM, the evolution of S follows the characteristic S-shape of logistic equations (Fig. 1). Further information on the calibration of CTEM is given in Section S3. A test of the calibration yields that the timescales produced by CTEM are generally matching the expected behaviour for AMAZ and PFTP (Fig. S3), but not for PFAT (Fig. S4). For PFAT we find that the carbon emissions are generally too low in 2100, however, this emission deficit is removed until 2300, where emissions of
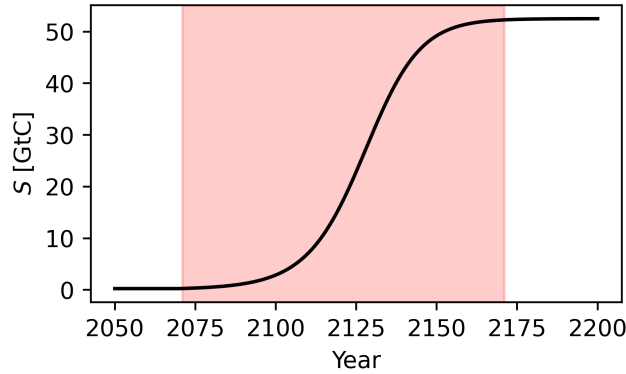
Figure 1. S for the calibration of the mean timescale of AMAZ (under SSP5-8.5). The red shaded area denotes the period over which 99% of the cumulative carbon emissions occur.

PFAT match the estimates. We regard this deviation to be acceptable, given the simplicity of our model approach (see Section S4 for further information).

2.3.1 Coupling to FaIR

CTEM is coupled to FaIR every timestep by adding E_{TE} to E_{SSP}. For each TE, we calculate E_{TE} from S as

$$E_{\text{TE}}(t) = S(t) - S(t-1).$$

The total carbon emissions E_{TE} are split up into CO_2 and CH_4 emissions for all three TEs. For PFAT, we assume that 20% of the carbon is emitted as CH_4, following Turetsky et al. (2020), while no CH_4 emissions are expected from AMAZ (Armstrong McKay et al., 2022). Quantifying the fraction of CH_4 emissions arising from PFTP is challenging due to the lack of previous model studies and limited process understanding. We rely on the 2D model study conducted by Schneider von Deimling et al. (2015), who report 40% of additional warming due to CH_4 emissions from the Yedoma deposits, which can be associated with PFTP. Since this amplification is within the uncertainty range of additional warming caused by CH_4 emissions from gradual permafrost thaw of $35 - 48\%$ for which 2.3% of the carbon is emitted as methane (Schuur et al., 2015), we assume that this fraction of CH_4 emissions also holds for PFTP. The annual CH_4 and CO_2 emissions of all three TEs are then added to $E_{\text{SSP}}(t)$ of the respective SSP and the sum is used to run the next timestep of FaIR, calculating $T(\bar{t})$ which is then used to force CTEM and so on.

To avoid double counting of carbon emissions, carbon emissions from the carbon TEs modelled by CTEM must not be included in FaIR. We can rule this possibility out, since carbon emissions from carbon TEs are neither accounted for by the CMIP6 models used to parameterize FaIR, nor of major importance for the observed warming signal used to constrain the parameter ensemble (See Section S6 for further explanation and references).
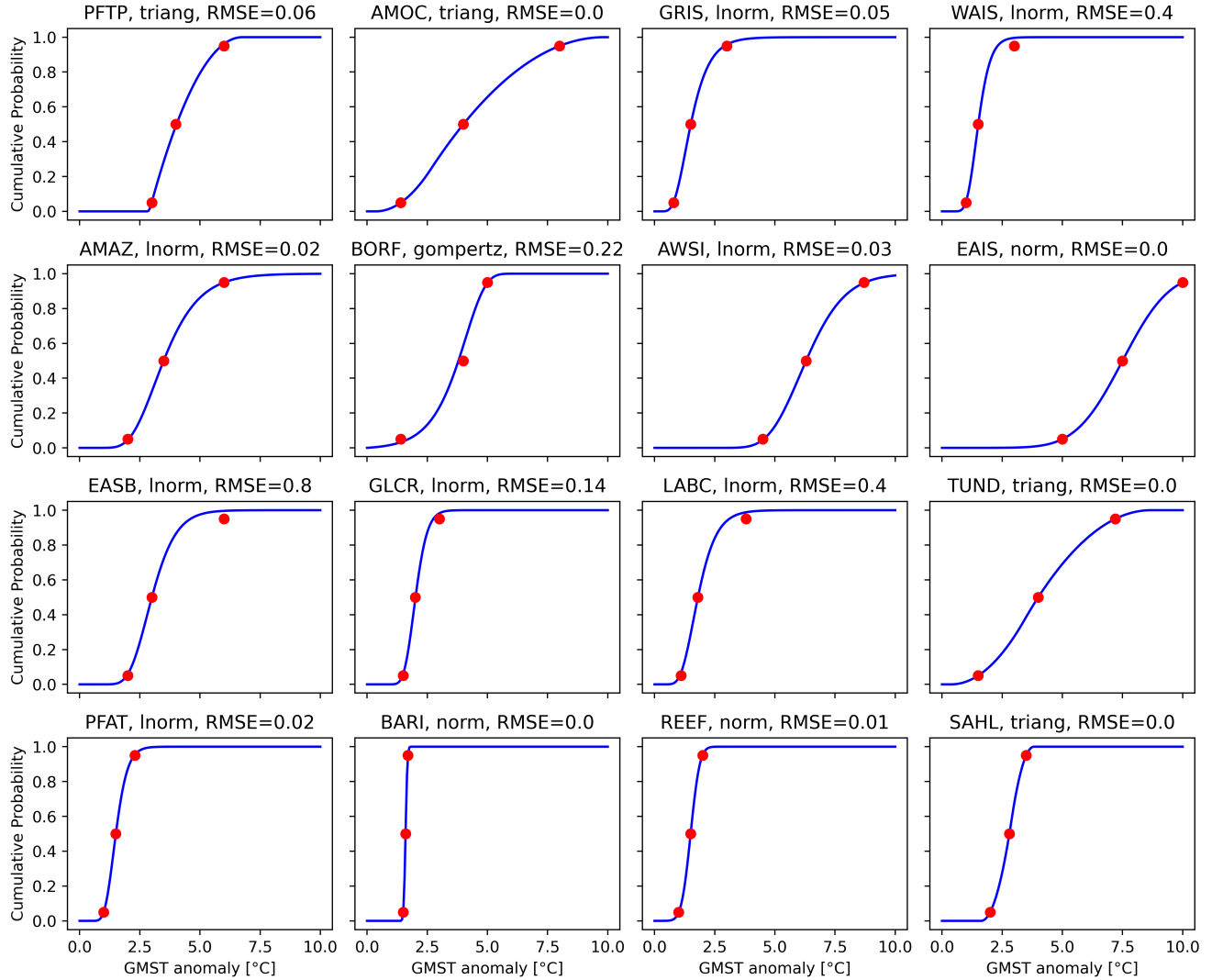
Figure 2. Cumulative distribution functions of P for all TEs, together with the RMSE between the given percentiles (red dots) and the actual percentiles of the respective distribution. The title states TE, distribution type and RMSE in °C.

2.4   Generation of Model Ensembles

We construct a coupled (FaIR coupled to CTEM) and an uncoupled (FaIR only) 5000 members model ensemble for SSP1-
2.6, SSP2-4.5, SSP3-7.0 and SSP5-8.5. Hereby, we follow a Monte Carlo scheme (Metropolis et al., 1953) to propagate the
uncertainties within FaIR and CTEM.

For the parameterization of FaIR, we randomly select 5000 members of its constrained parameter ensemble. We use the same parameter sample for FaIR in both the coupled and the uncoupled ensemble to make sure that changes in the climate response only arise from carbon emissions of the carbon TEs.

For the parameterization of CTEM and the calculation of triggering probabilities, we construct probability distributions of the respective parameters based on the estimates given in Table 1. From those probability distributions, we sample parameter values, employing Latin hypercube sampling (McKay et al., 1979).

To calculate the probability of triggering, we sample the uncertainty range of P for all TEs, again using the same parameter sample for both ensembles. For the sampling process of P, we infer probability distributions from the estimates in Table 1, deciding that the minimum estimate, the best estimate, and the maximum estimate should correspond to the 5th, the 50th and the 95th percentile of the respective probability distribution. To determine the probability distributions which best fits those percentiles, we use the "rriskDistributions" package (Belgorodski et al., 2017), which chooses out of 17 continuous probability distributions, minimizing the absolute difference between the given and the actual percentiles. We derive eight log-normal, four triangular, three normal and one Gompertz distribution (Fig. 2). While some distributions of P agree perfectly with the given percentiles (AMOC, EAIS, TUND, BARI, SAHL), others deviate substantially with RMSEs higher than 0.2°C (WAIS, BORF, EASB, LABC). In the case of WAIS, EASB, and LABC this deviation is mainly caused by too low values at the 95th percentile, which is reached at 2.3°C rather than 3°C for WAIS, 4.6°C rather than 6°C for EASB, and 3.1°C rather than 3.8°C for LABC. In the case of BORF, the relatively high RMSE is caused by a too high value at the 5th percentile (1.7°C rather than 1.4°C) and a too low value at the 50th percentile (3.8°C rather than 4°C), while the 95th percentile agrees well with the expected value (less than 0.02°C deviation). Even though the deviations between the given and the actual percentiles of those four TEs are significant, we regard them to be acceptable, given that they cannot be reduced with our methodology, meaning that other probability distributions would be needed to achieve this. However, it must be kept in mind that high probabilities of tipping might be reached at too low values of GMST for WAIS, EASB and LABC due to their imperfect probability distributions of P.

We now turn to the parameterization of CTEM. For the distribution of H for PFTP and AMAZ, we derive one log-normal distribution each, following the same approach as for the generation of probability distributions of P (Fig. S5). The impacts K of PFTP and AMAZ and the maximum impact K_{max} of PFAT are sampled from continuous uniform distributions, with the same probability for all values within the given ranges from Table 1 (Fig. S6). We regard this reasonable since Armstrong McKay et al. (2022) only give maximum and minimum values for those variables, and we do not have any additional information about their distribution. The feedback strengths F_{100} and F_{300} of PFAT are also sampled from continuous uniform distributions, with the same probability for all values within the given ranges from Table 1 (Fig. S7). Here, the same argument holds as for the selection of the distributions of K and K_{max}.

We assume that all parameters within the parameter set of CTEM are uncorrelated, except for F_{100} and F_{300}, which are correlated with a correlation coefficient of 1. The decision about the correlation of the parameters represents our understanding that there are no correlations, or at least no clear evidence for them, between the threshold temperatures, the timescales, or the impacts of AMAZ, PFAT and PFTP. The correlation between F_{100} and F_{300} is established since H of PFAT is included

in those parameters, and we assume that H is constant over time, e.g., a low feedback in 2100 associated with a high H also means low feedback in 2300 due to the same high H the emissions occur over.

2.5 Calculation of Tipping Probabilities

245 To calculate the probabilities of triggering any of the 16 TEs discussed in this study, we sample one value of P from the respective distribution (Fig. 2) for each TE and each ensemble member. If T of that ensemble member exceeds P, the TE is counted as triggered. In this manner, we derive the share of ensemble members in which a TE is triggered for each TE at all times. As all TEs discussed here are by definition irreversible on the considered timescale, the share of triggered TEs cannot decrease with time, even if T would decrease. The share of ensemble members with triggered TEs is then used to further
250 investigate the probabilities of triggering, e.g., by calculating the timing of the exceedance of certain share percentages.

2.6 Robustness of the Results

To examine whether an ensemble of size 5000 is sufficiently large to approximate the distributions of the output variables with our Monte Carlo approach, we create 20 coupled ensembles with 5000 members and run under SSP5-8.5, sampling uncertainties within FaIR and CTEM. As carbon emissions from CTEM are used to calculate T, which is also the final output
255 variable of FaIR, it includes uncertainties from all parameters and is hence expected to vary most between different ensembles. Therefore, we inspect the deviation of T between the 20 ensembles. While the 5th percentile and the mean of T are nearly equal for all ensembles, with standard deviations below 0.06°C at all times, the 95th percentile deviates slightly between the ensembles, with a standard deviation of up to 0.24°C (Fig. S8). Given the range of T between the 5th and the 95th percentile of ~ 11°C, we regard those deviations to be sufficiently small.

3 Carbon Emissions from Carbon Tipping Elements

The carbon emissions from carbon TEs increase from SSP1-2.6 to SSP5-8.5 (Fig. 3, Table 2). While zero carbon emissions from carbon TEs remain possible under SSP1-2.6, high carbon emissions become much more likely under SSP2-4.5, with the maximum emissions being nearly as high as under SSP5-8.5. This is a direct consequence of the probabilities of triggering carbon TEs. Under SSP1-2.6, triggering of PFAT occurs for 79% of the ensemble members, while triggering of AMAZ and
265 PFTP only happens for 13% and 5% respectively. Under SSP2-4.5, triggering probabilities are increased substantially, to 98% for PFAT, 53% for AMAZ and 37% for PFTP. This means that maximum carbon emissions with all three carbon TEs triggered become more likely under SSP2-4.5 compared to SSP1-2.6.

Even though the highest carbon emissions from carbon TEs occur under SSP3-7.0 and SSP5-8.5, they remain small compared to anthropogenic carbon emissions (Fig. 3). The 95th percentile of cumulative carbon emissions from carbon TEs only
270 reaches 14% of the cumulative anthropogenic carbon emissions in 2500 under SSP3-7.0, and 10% under SSP5-8.5. The relative contribution of carbon emissions from carbon TEs to the total carbon emissions increases towards lower emission scenarios.
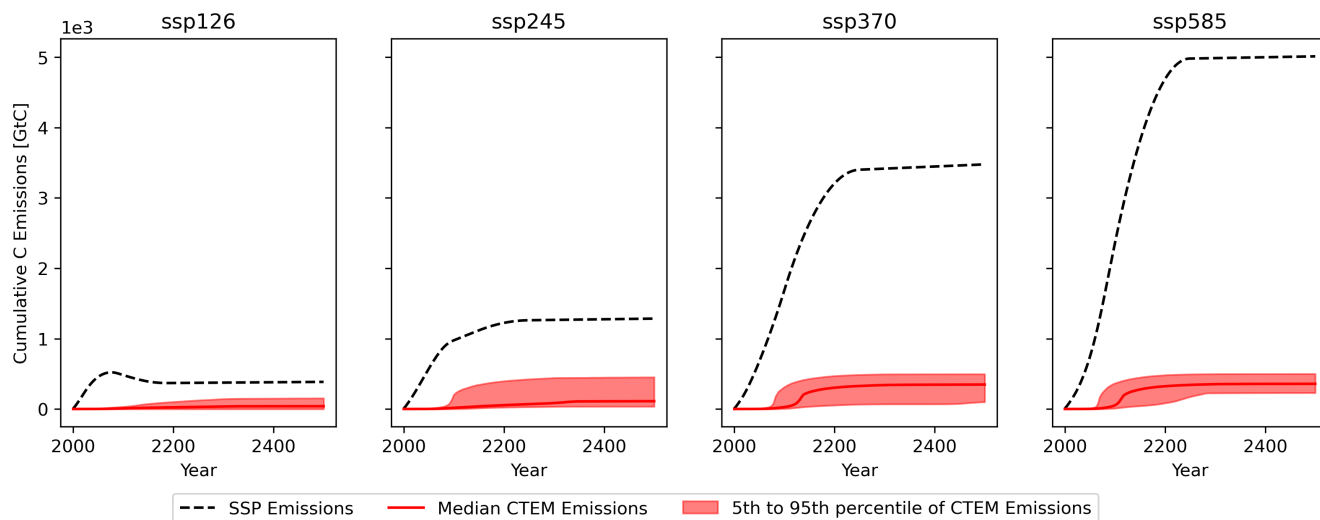
Figure 3. Cumulative carbon emissions from all SSP scenarios and the carbon TEs (modelled by CTEM) between 2000 and 2500.

Under SSP2-4.5 the 95th percentile of cumulative carbon emissions from carbon TEs reaches 35% of the cumulative anthropogenic carbon emissions in 2500, and 40% under SSP1-2.6.

Hence, SSP2-4.5 is special in the sense that maximum carbon emissions from carbon TEs are already possible and are large relative to the anthropogenic emissions.

4 Increase of Global Warming Caused by Carbon Tipping Elements

The carbon emissions from carbon TEs cause an increase in global warming (Fig. 4). Under SSP1-2.6, high temperature increases from carbon TEs are possible but not common, with the temperature distributions skewed towards higher values. No additional warming from carbon TEs remains possible under this scenario, with the 5th percentile being zero at all times (Table 2). Under SSP2-4.5, high impacts from carbon TEs become more common compared to SSP1-2.6. This is indicated by the median temperature increase, which reaches its maximum of 0.22°C in 2300 under SSP2-4.5, compared to only 0.08°C being reached in the same year under SSP1-2.6 (Table 2). Additional warming from carbon TEs becomes the default case under the high emission scenarios SSP3-7.0 and SSP5-8.5. The 5th percentile of the temperature increase is well above zero after 2100 for both scenarios and the median reaches 0.39°C and 0.4°C in 2300 and 2200 under SSP3-7.0 and SSP5-8.5 respectively (Table 2).

High additional warming from carbon TEs mostly occurs for ensemble members with a high climate sensitivity. This is indicated by the 95th percentile of the temperature distribution increasing more than all other percentiles if the warming from carbon TEs is included (Fig. 4). This effect is especially pronounced under SSP1-2.6 and SSP2-4.5.

		2050	2100	2200	2300	2400	2500
SSP1-2.6							
CO_2	[GtC]	1 (0-5)	8 (0-28)	20 (0-84)	30 (0-120)	32 (0-135)	32 (0-152)
CH_4	[$GtCH_4$]	0.3 (0-1.5)	2.5 (0-7.5)	6.3 (0-15.9)	9.6 (0-25.2)	10.4 (0-26.9)	10.5 (0-27.7)
dT	[°C]	0.01 (0-0.07)	0.06 (0-0.24)	0.08 (0-0.34)	0.1 (0-0.48)	0.06 (0-0.47)	0.06 (0-0.54)
SSP2-4.5							
CO_2	[GtC]	1 (0-5)	15 (1-148)	64 (19-323)	99 (28-359)	105 (29-365)	109 (39-368)
CH_4	[$GtCH_4$]	0.3 (0-1.7)	4.6 (0.3-13.5)	15.4 (6.3-32.9)	21.8 (9.1-43.3)	22.6 (9.5-44.6)	22.9 (9.5-45.1)
dT	[°C]	0.01 (0-0.07)	0.13 (0.01-0.59)	0.2 (0.06-0.85)	0.21 (0.06-0.91)	0.16 (0.03-0.89)	0.15 (0.03-0.91)
SSP3-7.0							
CO_2	[GtC]	1 (0-6)	33 (5-242)	284 (89-381)	317 (137-403)	322 (147-406)	323 (152-407)
CH_4	[$GtCH_4$]	0.3 (0-1.8)	7.9 (1.4-20)	29.3 (17-47.5)	35.1 (22.8-53.7)	35.6 (23.3-53.9)	35.9 (23.4-54)
dT	[°C]	0.01 (0-0.07)	0.25 (0.04-0.93)	0.39 (0.15-0.82)	0.31 (0.12-0.66)	0.27 (0.09-0.63)	0.26 (0.09-0.63)
SSP5-8.5							
CO_2	[GtC]	1 (0-8)	76 (13-282)	304 (136-389)	328 (233-408)	330 (243-410)	331 (246-411)
CH_4	[$GtCH_4$]	0.4 (0-2.2)	12.2 (3.1-26.2)	32 (20.5-50.5)	37.1 (24.1-54.3)	37.4 (24.3-54.6)	37.7 (24.3-54.7)
dT	[°C]	0.02 (0-0.09)	0.4 (0.09-1.11)	0.31 (0.13-0.64)	0.23 (0.1-0.52)	0.19 (0.08-0.47)	0.18 (0.08-0.47)

Table 2. Median and 5th – 95th percentile range of cumulative CO_2 and CH_4 emissions from the carbon TEs and the GMST increase (dT) caused by them. All quantities are calculated individually for each ensemble member as the increase caused by carbon TEs compared to the respective uncoupled ensemble member.
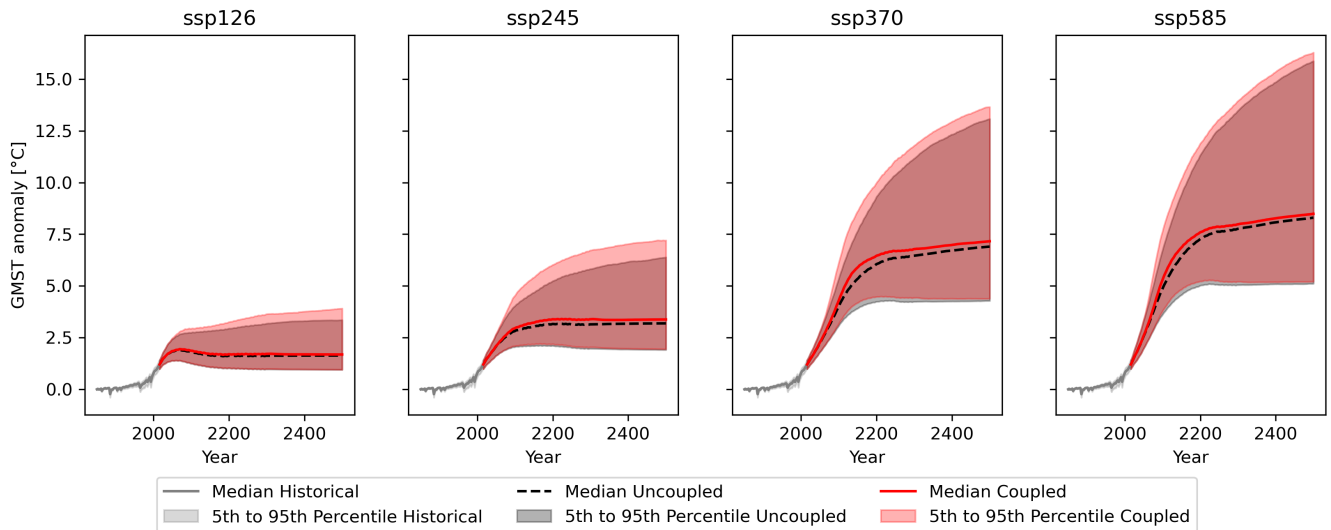
Figure 4. GMST relative to the 1850-1900 period of the coupled and the uncoupled ensemble, together with the historical evolution.

It is interesting to see that the highest long-term temperature increase from carbon TEs becomes possible under SSP2-4.5, with the 95th percentile reaching 0.91°C in 2500, and not under scenarios with higher anthropogenic emissions (Table 2). This is in contradiction to the cumulative CO_2 and CH_4 emissions from carbon TEs, which are higher under high emission scenarios than under SSP2-4.5. The reason for this behaviour is the implementation of the forcing relationship translating atmospheric CO_2 and CH_4 concentrations to radiative forcing developed by Etminan et al. (2016) and used in FaIR. It is approximated by a logarithmic and a square-root term for CO_2 and by a square-root term for CH_4, meaning that the effect of additional atmospheric concentrations of both GHGs on GMST is decreasing for higher atmospheric concentration levels. Therefore, the amount of carbon emissions from carbon TEs relative to the anthropogenic emissions is decisive to determine the additional warming from carbon TEs.

Nevertheless, it must be noted that the highest short-term temperature increase from carbon TEs becomes possible under the high emissions scenarios SSP3-7.0 and SSP5-8.5, with the upper end of the very likely range reaching 0.94°C and 1.11°C in 2100 under SSP3-70 and SSP5-8.5 respectively. This can be linked to high CH_4 emissions from fast PFAT degradation due to rapidly increasing temperatures, which leads to peaks in the atmospheric CH_4 concentration anomaly around 2100 (Fig. S9).

The temperature increase from carbon TEs occurs earlier under high emission scenarios (Table 2), which can be explained by threshold temperatures of the carbon TEs being crossed earlier under those scenarios, as the general temperature increase is faster (Fig. 4). Interestingly, the median temperature increase from carbon TEs is declining towards the end of the model period under all SSPs (Table 2). This can be linked to the decreasing atmospheric methane concentrations (Fig. S9).

When comparing the different SSPs, it becomes evident that high temperature increases from carbon TEs are possible but rare under low emission scenarios, and become more frequent but less strong compared to the anthropogenic warming under high emission scenarios (Table 2 and Fig. 4). This means that if anthropogenic carbon emissions can be limited to levels comparable to SSP1-2.6, there remains a risk that the warming might be substantially increased by triggering carbon TEs. On the other hand, if anthropogenic emissions keep increasing like under SSP5-8.5 warming will almost certainly be amplified by carbon TEs, however, this additional warming will remain small compared to the anthropogenic warming. On average, the additional warming from carbon TEs is low compared to the anthropogenic warming and the risk for high temperature increases is limited. This is indicated by the median temperature increase from carbon TEs always remaining at least one order of magnitude smaller than the median anthropogenic warming (Table 2 and Fig. 4).

5   Probabilities of Triggering Climate Tipping Elements

We now turn to the probabilities of triggering any of the 16 TEs proposed by Armstrong McKay et al. (2022) (Table 1), and how those probabilities are increased by the additional warming from carbon TEs. To compare those probabilities among the SSPs, we focus on the crossing of 50% probability, where triggering becomes more likely than not.

The effect of carbon TEs on the probabilities of triggering TEs under the different SSP scenarios is clearly visible, with triggering getting more likely earlier if carbon emissions from carbon TEs are included (Fig. 5). On average, TEs become more likely than not to be triggered 6.6 years earlier if carbon emissions from carbon TEs are included. This effect becomes
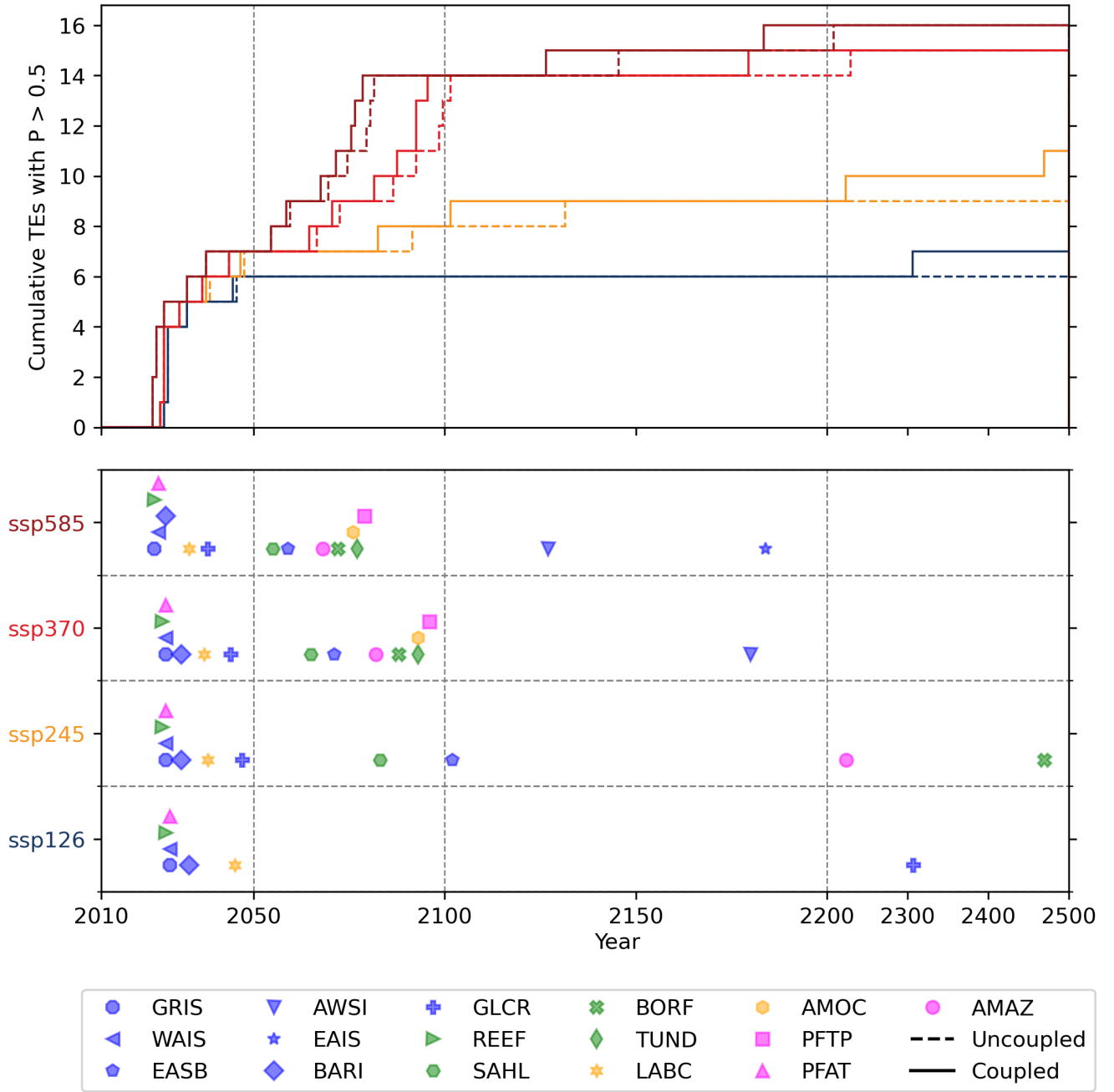
Figure 5. Cumulative number of TEs with a more than 50% probability (P) of getting triggered for the Tier1 SSP scenarios from the coupled and the uncoupled ensemble (upper row) and symbols of the triggered TEs corresponding to the increase of cumulative TEs in the coupled ensemble (lower row). Carbon TEs are marked with pink symbols, whereas the other TEs are marked in the colours suggested by Armstrong McKay et al. (2022), with blue for cryosphere, green for biosphere and orange for atmospheric or oceanic circulations.

more pronounced towards the end of the prediction period, since GMST is generally increasing slower at that time, which means it takes longer for the uncoupled ensemble to reach the same temperatures as the coupled ensemble (Fig. 4). Especially TEs within the cryosphere will become more likely than not to be triggered decades earlier, if carbon emissions from carbon TEs are included. EAIS and AWSI cross the 50% probability of triggering 25 years and 19 years earlier respectively under SSP5-8.5, AWSI crosses it 50 years earlier under SSP3-7.0, and EASB crosses it 30 years earlier under SSP2-4.5 (Fig. 5). As we do not consider any interactions between the TEs apart from the increase in GMST from carbon TEs, the fact that crossing of a certain probability level is achieved significantly earlier for some TEs if carbon emissions from carbon TEs are included is solely caused by a favourable combination of the threshold temperature distribution and the maximum temperatures reached under the respective SSP and should therefore not be over interpreted.

Even though additional probability of triggering caused by carbon emissions from carbon TEs clearly exists, it remains small compared to the probability of triggering caused by anthropogenic carbon emissions. Only three TEs become more likely than not to be triggered in addition to the uncoupled ensemble due to the inclusion of carbon TEs in the sum over all SSPs (Fig. 5). Carbon TEs do not cause high enough temperature increases to induce rapid triggering of multiple TEs following the tipping of the carbon TEs. Partly, this might be due to the fact that PFTP, which causes the highest carbon emissions of all carbon TEs, is one of the last TEs to be triggered and hence has little potential to cause earlier triggering of other TEs (Fig. 5). Moreover, even if all carbon TEs are extremely likely to be triggered, they only cause an increase of GMST of up to 0.4°C in the median under SSP5-8.5, which is too small to achieve crossing of multiple TE threshold temperatures (Table 2).

For the exceedance of the 50% probability of triggering, we observe clustering of the TEs, which has the potential to occur earlier if carbon emissions from carbon TEs are included. The first cluster consisting of five TEs (GRIS, WAIS, REEF, PFAT, and BARI) becomes more likely than not to be triggered by 2033, regardless of the emission scenario or whether carbon emissions from carbon TEs are included or not (Fig. 5). LABC and GLCR also exceed the 50% probability of being triggered before 2050 under SSP2-4.5, SSP3-7.0 and SSP5-8.5. A second cluster of seven TEs (SAHL, EASB, AMAZ, BORF, AMOC, TUND, and PFTP) crosses the 50% probability of triggering between 2050 and 2100 under SSP5-8.5 and SSP3-7.0. This can be partly avoided under SSP2-4.5 with only SAHL and EASB and if carbon emissions from carbon TEs are included also AMAZ and BORF becoming more likely than not to be triggered until 2500. Under SSP1-2.6, none of the TEs from the third cluster become more likely to be triggered than not, independent of carbon emissions from the carbon TEs. The two remaining

	Probability of Triggering [%]	Probability Increase from Carbon TEs [pp]
SSP1-2.6	37	2.2
SSP2-4.5	64	3.3
SSP3-7.0	91	1.0
SSP5-8.5	95	0.5

Table 3. Probability of triggering averaged over all TEs in 2500 and its increase due to additional warming caused by carbon emissions from carbon TEs in percent points (pp).
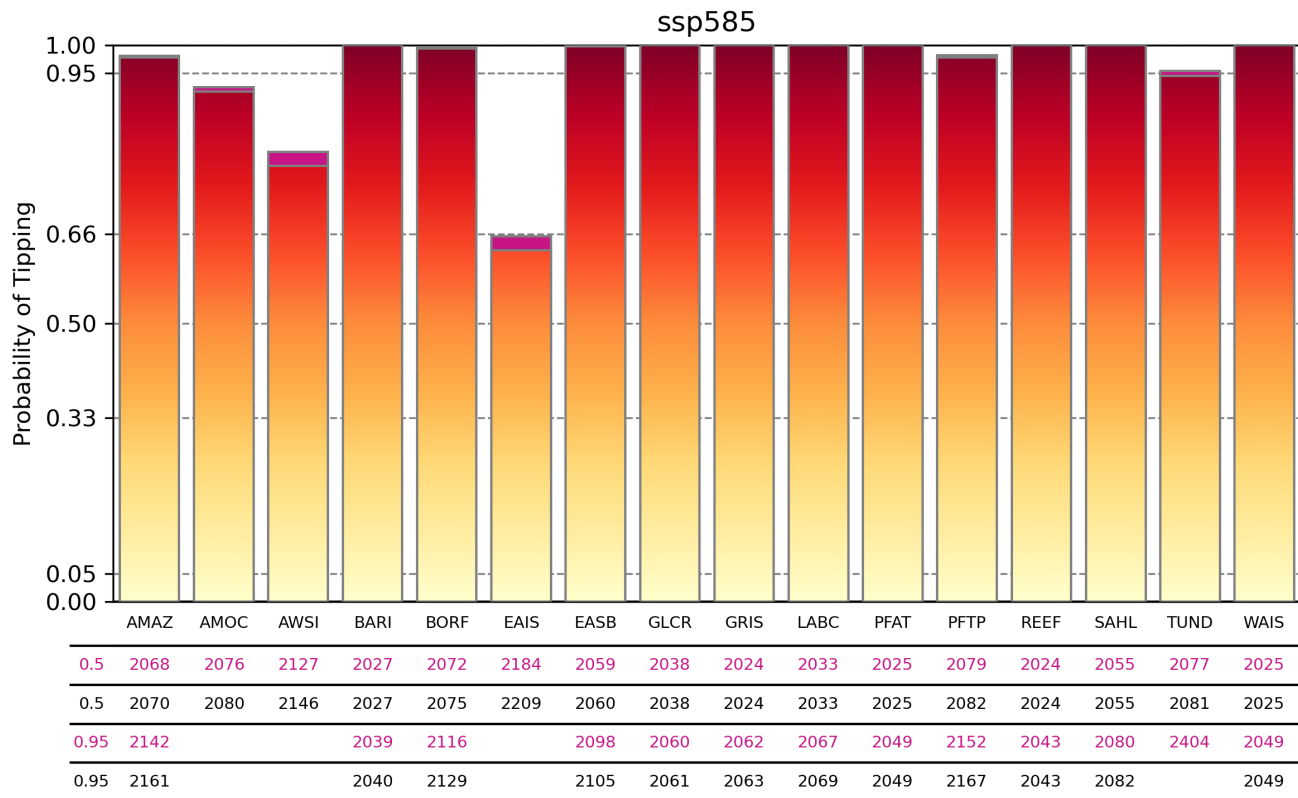
Figure 6. Probabilities of triggering the TEs by 2500 under SSP5-8.5. Additional probabilities from the carbon TEs are marked in purple. The table underneath states the years in which the 50% and 95% probability is crossed, with purple including carbon emissions from carbon TEs and black not.

TEs AWSI and EAIS do also exceed the 50% probability of being triggered under SSP5-8.5 until 2300, while this is only the case for AWSI under SSP3-7.0. Hence, all 16 TEs are more likely than not to be triggered by 2500 under SSP5-8.5, 15 under SSP3-70, eleven (nine) under SSP2-4.5, and seven (six) under SSP1-2.6 including (not including) the carbon emissions from carbon TEs.

While the above inspection of the 50% probability level is especially valuable to understand the timing of triggering TEs, a more thorough analysis of the triggering probabilities is needed to fully understand how the risk of triggering TEs changes for the different SSPs. We turn to this part now. To compare the general risk of triggering TEs and how it is amplified by carbon TEs, we calculate average triggering probabilities at the end of our model period in 2500 (Table 3). Unsurprisingly, they increase from SSP1-2.6 to SSP5-8.5.

Under SSP5-8.5, the probability of triggering is above 95% for most TEs, and only the probability for triggering EAIS remains just below 66% (Fig. 6). The probabilities of triggering are reduced slightly under SSP3-7.0, but the general picture

	AMAZ	AMOC	AWSI	BARI	BORF	EAIS	EASB	GLCR	GRIS	LABC	PFAT	PFTP	REEF	SAHL	TUND	WAIS
0.5	2224			2031	2470		2102	2047	2027	2038	2027		2026	2083		2027
0.5				2031			2132	2048	2027	2039	2027		2026	2092		2027
0.95				2049					2187		2073		2057			2072
0.95				2050							2073		2058			2076
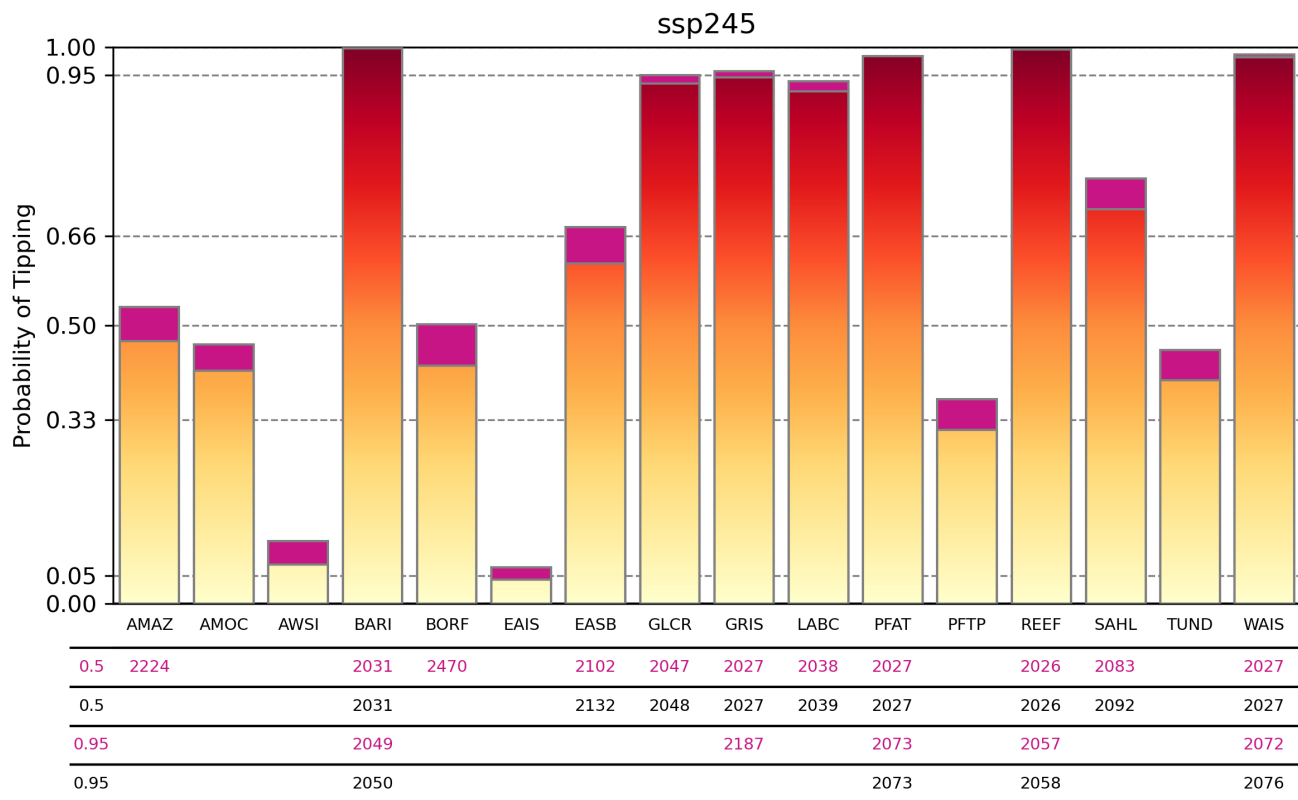
Figure 7. Probabilities of triggering the TEs by 2500 under SSP2-4.5. Additional probabilities from the carbon TEs are marked in purple. The table underneath states the years in which the 50% and the 95% probability are crossed, with purple including carbon emissions from carbon TEs and black not.

remains the same (Fig. S10). Interestingly, the additional probability of triggering TEs is lowest under the two high emission scenarios (Table 3). Temperatures well above the threshold temperatures of most TEs are reached even without the effect of carbon TEs, hence, their impact on triggering probabilities is almost negligible.

Under SSP2-4.5 the probabilities of triggering vary strongly between different TEs. The four TEs BARI, REEF, PFAT, and WAIS are triggered with more than 95% probability under SSP2-4.5, with GRIS crossing 95% probability as well if carbon emissions from carbon TEs are included (Fig. 7). GLCR, LABC, SAHL and, if carbon emissions from carbon TEs are included, EASB are triggered with more than 66% probability. Additional carbon emissions from carbon TEs also lead to AMAZ and BORF becoming more likely than not to be triggered. Only AWSI, EAIS, and, if carbon emissions from carbon TEs are not accounted for, PFTP remain below 33% probability of getting triggered, as TUND and AMOC are exceeding 33% probability in both ensembles. Triggering of EAIS remains below 5% probability only if carbon emissions from the carbon TEs are not included.
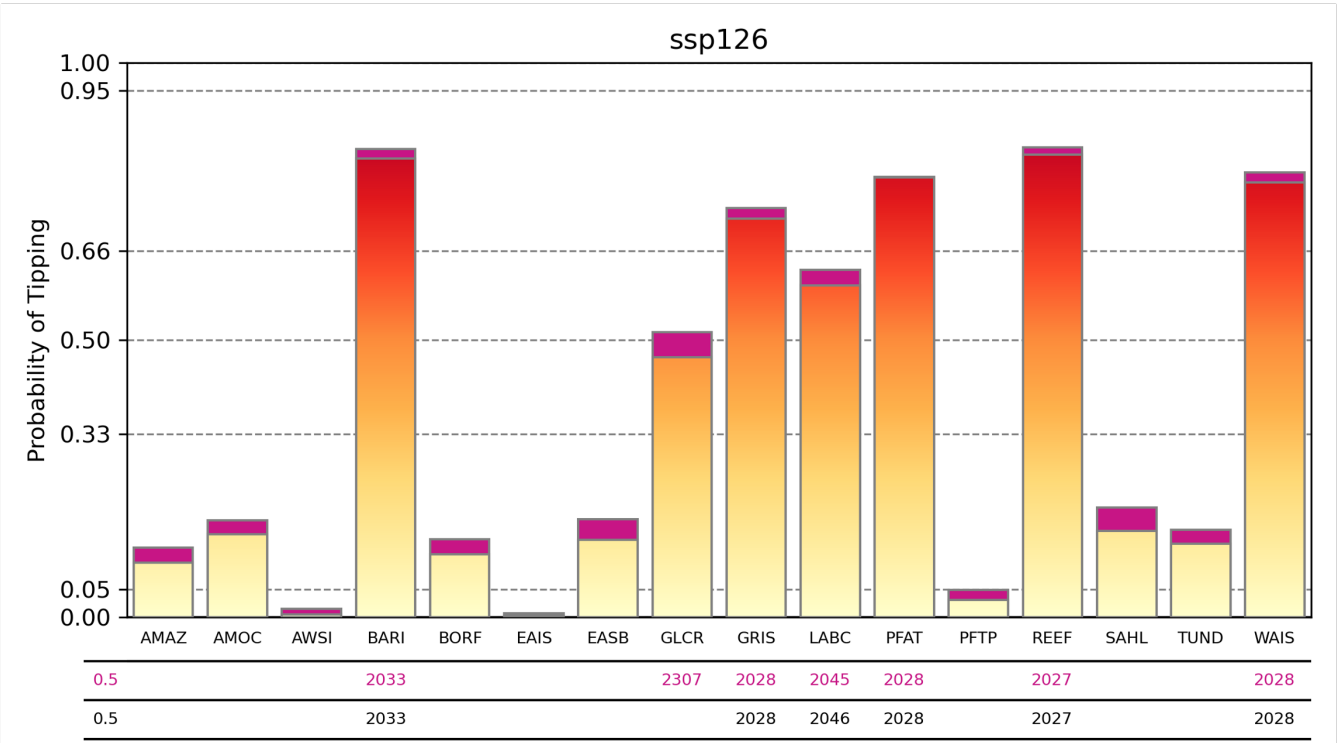
Figure 8. Probabilities of triggering the TEs by 2500 under SSP1-2.6. Additional probabilities from the carbon TEs are marked in purple. The table underneath states the years in which the 50% probability is crossed, with purple including carbon emissions from carbon TEs and black not.

370   The increase in probabilities of triggering caused by carbon emissions from carbon TEs is highest under SSP2-4.5 (Table 3). This matches our finding that the highest long-term temperature increase from carbon TEs is also possible under this scenario (Table 2).

Moving from SSP2-4.5 to SSP1-2.6 reduces the probability of triggering multiple TEs significantly, namely by 27 pp (Table 3). No TE exceeds 95% probability of getting triggered under SSP1-2.6. However, the five TEs PFAT, REEF, GRIS, WAIS,

375   and BARI are still triggered with a probability higher than 66% regardless of carbon emissions from carbon TEs (Fig. 8). The probability for triggering LABC is still higher than 50%, which is also true for GLCR if carbon emissions from carbon TEs are included. For all other TEs the probability of triggering remains below 33%, and even below 5% for AWSI, EAIS and PFTP under SSP1-2.6. The additional probability of triggering from carbon TEs is also reduced by 1.1 pp compared to SSP2-4.5 (Table 3).

6 Discussion

With CTEM we introduce a simplistic model which is able to represent carbon emissions from the three carbon TEs PFAT, PFTP and AMAZ in line with the estimates from Armstrong McKay et al. (2022). However, the impacts from the carbon TEs estimated in this study remain somewhat speculative, as there is only limited confidence about the actual existence of tipping points within the carbon TEs, with low confidence for PFTP and medium confidence for PFAT and AMAZ (Table 1). The distinction between PFGT, PFAT and PFTP made by Armstrong McKay et al. (2022) for permafrost thaw also remains questionable. Most studies, including the latest IPCC report, assume that permafrost thaw can be divided into gradual and abrupt thaw processes, corresponding to PFGT and PFAT, and do not mention permafrost collapse due to compost bomb instabilities (PFTP) (e.g. Canadell et al., 2021; Turetsky et al., 2020; Schuur et al., 2015; Wang et al., 2023). Since PFTP causes the highest carbon emissions out of all three carbon TEs with up to 250 GtC (Table 1), the impact of tipping elements within the carbon cycle will be less severe than found in this study if PFTP does not include a tipping point.

Yet, additional carbon emissions released by PFGT under continued global warming of up to 260 GtC (Table 1) need to be expected, which are not considered in this study. One reason to exclude PFGT is that it is not assumed to include tipping points, but to be a threshold-free feedback to global warming (Armstrong McKay et al., 2022). Furthermore, sophisticated models of PFGT already exist (e.g. Gasser et al., 2018; Burke et al., 2020), hence it would not be appropriate to represent PFGT with a simple conceptual model like CTEM.

It is challenging to compare the carbon emissions from carbon TEs identified by us to other studies, as this is to the best of our knowledge the first study to investigate the impact of all TEs within the carbon cycle. Other studies are only analysing single TEs, e.g., Cox et al. (2004); Parry et al. (2022) for AMAZ or Schneider von Deimling et al. (2015); Gasser et al. (2018) for permafrost thaw as a whole. Since the individual carbon emissions from the carbon TEs modelled by CTEM are based on the estimates of Armstrong McKay et al. (2022), we would only reproduce their analysis by comparing our individual carbon emission estimates to the literature. Nevertheless, it must be noted that even though the uncertainty ranges of the carbon impacts identified by Armstrong McKay et al. (2022) based on numerous studies are large (factor two for PFTP and AMAZ, factor three for PFAT), they do not include all estimates from the literature. Especially the lower bounds of AMAZ and PFTP are questionable. Carbon emissions from the Yedoma region, which make up for the major part of PFTP emissions, of only 23 GtC in 2300 under RCP5-8.5 have been found by an observations-based modelling study (Schneider von Deimling et al., 2015). This is much lower than the minimum carbon emissions of 100 GtC from the Yedoma region assumed by Armstrong McKay et al. (2022), which led to an estimated minimum impact of PFTP of 125 GtC. The minimum impact of 30 GtC for AMAZ might also be too high since no substantial carbon loss from AMAZ is observable in CMIP6 models, even if localized dieback occurs (Parry et al., 2022). Given that the emission estimates from Armstrong McKay et al. (2022) used to parameterize CTEM seem to be on the high side compared to other studies, we are confident about our finding that the warming caused by carbon TEs on average remains small compared to the anthropogenic warming.

Our estimates of probabilities of triggering are generally higher than the values reported by Kriegler et al. (2009), which have found much use in the climate tipping points literature (e.g. Lontzek et al., 2015; Cai et al., 2015, 2016). They provide

ranges of probabilities of triggering for the year 2200 under three warming scenarios: a low temperature corridor comparable
to SSP1-1.9, a medium temperature corridor comparable to SSP2-4.5 and a high temperature corridor comparable to SSP3-7.0.
For the medium temperature corridor, Cai et al. (2016) infer mean probabilities of triggering from the ranges given in Kriegler
et al. (2009) of 22% for AMOC, 52% for GRIS, 34% for WAIS, and 48% for AMAZ, which can be compared to our estimates
in 2200 under SSP2-4.5 (without carbon TEs impacts) of 38% for AMOC, 94% for GRIS, 98% for WAIS, and 43% for AMAZ
(Fig. S12).

Those deviations can be explained by the new scientific literature being published since Kriegler et al. (2009), which provides
the basis for the threshold temperature estimates from Armstrong McKay et al. (2022) our calculation of triggering probabilities
is largely based on. The increased triggering probability for AMOC can be linked to various studies reporting unrealistic
stability of AMOC in GCMs (e.g. Liu et al., 2017), together with empirical evidence for loss of stability of AMOC (Boers,
2021). New indications for the proximity of a tipping point for GRIS are also derived from observations of ice loss (King et al.,
2020; Boers and Rypdal, 2021), with recent modelling studies confirming this (Van Breedam et al., 2020; Robinson et al.,
2012). Loss of WAIS is becoming observable (Shepherd et al., 2019) and a tipping point might already be crossed with several
glaciers in the Amundsen Sea currently undergoing marine ice sheet instability (Rignot et al., 2014).

Even though we find an increase in the probabilities of triggering caused by the additional carbon emissions from carbon
TEs, this impact is not strong enough to trigger any tipping cascades and remains small compared to the scenario–dependence
of tipping probabilities. Additional carbon emissions from carbon TEs only cause existing clusters of TEs to be triggered
earlier (Fig. 5). Even under SSP2-4.5, which features the highest long-term increase in temperature of up to 0.91°C due to
carbon emissions from carbon TEs, the additional probability of triggering caused by this temperature increase is only 3.3 pp
on average and only two TEs become more likely than not to be triggered if this temperature increase is accounted for. Despite
our finding that the impact from carbon TEs alone is too small to trigger tipping cascades, tipping cascades might still emerge
as major physical interactions between TEs aside from carbon emissions are not accounted for in this study (Wunderling et al.,
2021).

A shortcoming of our calculation of triggering probabilities is that we do not allow for temporal overshoot of threshold
temperatures but count a tipping element as triggered once its threshold temperature is crossed. For how long the thresh-
old temperature can be exceeded without triggering depends on the internal timescale of the TE, and is therefore especially
pronounced for TEs within the cryosphere (Ritchie et al., 2021). Therefore, we might be overestimating probabilities of trig-
gering for cryospheric TEs under SSP1-2.6, which features a slight temperature overshoot. Further constraining the internal
timescales of TEs could be an interesting topic of future research and would enable studies like ours to include the possibility
for overshoot.

It must also be noted that our findings critically depend on the assessment of climate tipping points by Armstrong McKay
et al. (2022). However, we believe that this study best summarizes the current state of knowledge about climate tipping points,
relying on more than 300 references. Narrowing the uncertainty range of threshold temperatures is an enormous task for future
research, which would allow for more precise statements about the probability of triggering climate TEs.

7 Conclusions

We developed a simple model framework to explore the probabilities of triggering climate TEs and how they are amplified by carbon emissions from carbon TEs under various SSPs.

We show that the additional carbon emissions from carbon TEs increase the risk for high temperature pathways, especially under SSPs with comparably low anthropogenic carbon emissions. On average, however, the additional warming from carbon TEs remains low compared to the anthropogenic warming. Therefore, the probability of triggering climate TEs is to first order determined by the emission scenario and not by whether carbon TEs are triggered or not. Consistent with this, we also don't see any tipping cascades being triggered by carbon TEs.

Current policies, steering towards a pathway comparable to SSP2-4.5 (Climate Action Tracker, 2022; United Nations Environment Programme, 2022; Meinshausen et al., 2022), are highly unsafe with regard to triggering climate tipping points. Triggering of multiple TEs is likely under SSP2-4.5 with 64% probability of triggering on average over all 16 TEs in 2500. The temperature increase from carbon TEs increases this number by a 3.3 pp, which is the highest probability increase caused by carbon TEs among all SSPs. This is in line with the highest long-term temperature increase caused by carbon TEs becoming possible under SSP2-4.5, with values reaching from 0.03°C to 0.91°C in 2500 (5th to 95th percentile range). Moving from SSP2-4.5 to SSP1-2.6 reduces the probability of triggering TEs substantially, with an average probability of triggering until 2500 of 37% under SSP1-2.6. The impact of carbon TEs is also less severe under this scenario, ranging from 0°C to 0.54°C in 2500, which leads to an increase in the average probability of triggering of 2.2 pp.

The probabilities of triggering climate TEs derived by us are higher than the estimates from the often cited expert elicitation conducted by (Kriegler et al., 2009). This is explained by recent evidence for the proximity of climate tipping points, leading to low estimates of the respective threshold temperatures.

If the risk of triggering TEs is to be reduced, rapid action is needed to reduce greenhouse gas emissions, since climate tipping points are already close, and it will be decided within the coming decades if they will be crossed or not.

Code and data availability. The code to reproduce the model output and the plots is available from https://github.com/JakobDeutloff/TP_paper and archived under https://zenodo.org/records/10136536 (Deutloff, 2023b). The model output and the parameter sets used to produce it are archived under https://zenodo.org/records/10136870 (Deutloff, 2023a).

Author contributions. JD designed the study and wrote the paper with input from both co-authors. JD performed and analysed the model simulations and prepared all figures and tables. HH co-designed the sampling strategy, and contributed to the discussion of the method and the results. TL contributed to the research design and the discussion of the methods and the results.

Competing interests. Tim Lenton is an editor of the special issue on tipping points in the Anthropocene. The peer-review process was guided by an independent editor, and the authors have also no other competing interests to declare.

Acknowledgements. The authors would like to thank David Armstrong McKay and Jesse Abrams for the discussion of ideas and valuable suggestions for the model development. The Global Systems Institute, where the major part of this research was conducted, was supported by the Bezos Earth Fund.

480

References

Armstrong McKay, D. I., Staal, A., Abrams, J. F., Winkelmann, R., Sakschewski, B., Loriani, S., Fetzer, I., Cornell, S. E., Rockström, J., and Lenton, T. M.: Exceeding 1.5°C global warming could trigger multiple climate tipping points, Science (New York, N.Y.), 377, eabn7950, https://doi.org/10.1126/science.abn7950, 2022.

485 Belgorodski, N., Greiner, M., Tolksdorf, K., Schueller, K., Flor, M., and Göhring, L.: rriskDistributions, https://CRAN.R-project.org/package=rriskDistributions, 2017.

Boers, N.: Observation-based early-warning signals for a collapse of the Atlantic Meridional Overturning Circulation, Nature Climate Change, 11, 680–688, https://doi.org/10.1038/s41558-021-01097-4, 2021.

Boers, N. and Rypdal, M.: Critical slowing down suggests that the western Greenland Ice Sheet is close to a tipping point, Proceedings of
490 the National Academy of Sciences of the United States of America, 118, 1–7, https://doi.org/10.1073/pnas.2024192118, 2021.

Burke, E. J., Zhang, Y., and Krinner, G.: Evaluating permafrost physics in the Coupled Model Intercomparison Project 6 (CMIP6) models and their sensitivity to climate change, Cryosphere, 14, 3155–3174, https://doi.org/10.5194/tc-14-3155-2020, 2020.

Cai, Y., Judd, K. L., Lenton, T. M., Lontzek, T. S., and Narita, D.: Environmental tipping points significantly affect the cost-benefit assessment of climate policies, Proceedings of the National Academy of Sciences, 112, 4606–4611, https://doi.org/10.1073/pnas.1503890112, 2015.

495 Cai, Y., Lenton, T. M., and Lontzek, T. S.: Risk of multiple interacting tipping points should encourage rapid CO2 emission reduction, Nature Climate Change, 6, 520–525, https://doi.org/10.1038/nclimate2964, 2016.

Canadell, J., Monteiro, P., Costa, M., Cotrim da Cunha, L., Cox, P., Eliseev, A., Henson, S., Ishii, M., Jaccard, S., Koven, C., Lohila, A., Patra, P., Piao, S., Rogelj, J., Syampungani, S., Zaehle, S., and Zickfeld, K.: Global Carbon and other Biogeochemical Cycles and Feedbacks, in: Climate Change 2021: The Physical Science Basis. Contribution of Working Group I to the Sixth Assessment Re-
500 port of the Intergovernmental Panel on Climate Change, edited by Masson-Delmotte, V., Zhai, P., Pirani, A., Connors, S., Péan, C., Berger, S., Caud, N., Chen, Y., Goldfarb, L., Gomis, M., Huang, M., Leitzell, K., Lonnoy, E., Matthews, J., Maycock, T., Waterfield, T., Yelekçi, O., Yu, R., and Zhou, B., p. 673–816, Cambridge University Press, Cambridge, United Kingdom and New York, NY, USA, https://doi.org/10.1017/9781009157896.007, 2021.

Chen, D., Rojas, M., Samset, B., Cobb, K., Diongue Niang, A., Edwards, P., Emori, S., Faria, S., Hawkins, E., Hope, P., Huybrechts, P.,
505 Meinshausen, M., Mustafa, S., Plattner, G.-K., and Tréguier, A.-M.: Framing, Context, and Methods, in: Climate Change 2021: The Physical Science Basis. Contribution of Working Group I to the Sixth Assessment Report of the Intergovernmental Panel on Climate Change, edited by Masson-Delmotte, V., Zhai, P., Pirani, A., Connors, S., Péan, C., Berger, S., Caud, N., Chen, Y., Goldfarb, L., Gomis, M., Huang, M., Leitzell, K., Lonnoy, E., Matthews, J., Maycock, T., Waterfield, T., Yelekçi, O., Yu, R., and Zhou, B., p. 147–286, Cambridge University Press, Cambridge, United Kingdom and New York, NY, USA, https://doi.org/10.1017/9781009157896.003, 2021.

510 Climate Action Tracker: The CAT Thermometer, https://climateactiontracker.org/global/cat-thermometer/, 2022.

Cox, P. M., Betts, R. A., Collins, M., Harris, P. P., Huntingford, C., and Jones, C. D.: Amazonian forest dieback under climate-carbon cycle projections for the 21st century, Theoretical and Applied Climatology, 78, 137–156, https://doi.org/10.1007/s00704-004-0049-4, 2004.

Deutloff, J.: Ensemble Outputs and Triggering Probabilities (Dataset), https://doi.org/10.5281/zenodo.8099907, 2023a.

Deutloff, J.: Model Code and Evaluation Scripts (Version 1.2), https://doi.org/10.5281/zenodo.8099987, 2023b.

515 Etminan, M., Myhre, G., Highwood, E. J., and Shine, K. P.: Radiative forcing of carbon dioxide, methane, and nitrous oxide: A significant revision of the methane radiative forcing, Geophysical Research Letters, 43, 12,614–12,623, https://doi.org/10.1002/2016GL071930, _eprint: https://onlinelibrary.wiley.com/doi/pdf/10.1002/2016GL071930, 2016.

Forster, P., Storelvmo, T., Armour, K., Collins, W., Dufresne, J.-L., Frame, D., Lunt, D., Mauritsen, T., Palmer, M., Watanabe, M., Wild, M., and Zhang, H.: The Earth's Energy Budget, Climate Feedbacks, and Climate Sensitivity, in: Climate Change 2021: The Physical Science Basis. Contribution of Working Group I to the Sixth Assessment Report of the Intergovernmental Panel on Climate Change, edited by Masson-Delmotte, V., Zhai, P., Pirani, A., Connors, S., Péan, C., Berger, S., Caud, N., Chen, Y., Goldfarb, L., Gomis, M., Huang, M., Leitzell, K., Lonnoy, E., Matthews, J., Maycock, T., Waterfield, T., Yelekçi, O., Yu, R., and Zhou, B., p. 923–1054, Cambridge University Press, Cambridge, United Kingdom and New York, NY, USA, https://doi.org/10.1017/9781009157896.009, 2021.

Gasser, T., Kechiar, M., Ciais, P., Burke, E. J., Kleinen, T., Zhu, D., Huang, Y., Ekici, A., and Obersteiner, M.: Path-dependent reductions in CO2 emission budgets caused by permafrost carbon release, Nature Geoscience, 11, 830–835, https://doi.org/10.1038/s41561-018-0227-0, 2018.

Gidden, M. J., Riahi, K., Smith, S. J., Fujimori, S., Luderer, G., Kriegler, E., Van Vuuren, D. P., Van Den Berg, M., Feng, L., Klein, D., Calvin, K., Doelman, J. C., Frank, S., Fricko, O., Harmsen, M., Hasegawa, T., Havlik, P., Hilaire, J., Hoesly, R., Horing, J., Popp, A., Stehfest, E., and Takahashi, K.: Global emissions pathways under different socioeconomic scenarios for use in CMIP6: A dataset of harmonized emissions trajectories through the end of the century, Geoscientific Model Development, 12, 1443–1475, https://doi.org/10.5194/gmd-12-1443-2019, 2019.

Guetschow, J., Jeffery, M. L., Gieseke, R., Gebel, R., Stevens, D., Krapp, M., and Rocha, M.: The PRIMAP-hist national historical emissions time series, Earth System Science Data, 8, 571–603, https://doi.org/10.5194/essd-8-571-2016, 2016.

Hoesly, R. M., Smith, S. J., Feng, L., Klimont, Z., Janssens-Maenhout, G., Pitkanen, T., Seibert, J. J., Vu, L., Andres, R. J., Bolt, R. M., Bond, T. C., Dawidowski, L., Kholod, N., Kurokawa, J.-I., Li, M., Liu, L., Lu, Z., Moura, M. C. P., O'Rourke, P. R., and Zhang, Q.: Historical (1750–2014) anthropogenic emissions of reactive gases and aerosols from the Community Emissions Data System (CEDS), Geoscientific Model Development, 11, 369–408, https://doi.org/10.5194/gmd-11-369-2018, 2018.

IPCC: Summary for Policymakers, p. 3-32, Cambridge University Press, Cambridge, United Kingdom and New York, NY, USA, https://doi.org/10.1017/9781009157896.001, 2021.

Khvorostyanov, D. V., Ciais, P., Krinner, G., and Zimov, S. A.: Vulnerability of east Siberia's frozen carbon stores to future warming, Geophysical Research Letters, 35, 1–5, https://doi.org/10.1029/2008GL033639, 2008.

King, M. D., Howat, I. M., Candela, S. G., Noh, M. J., Jeong, S., Noël, B. P. Y., van den Broeke, M. R., Wouters, B., and Negrete, A.: Dynamic ice loss from the Greenland Ice Sheet driven by sustained glacier retreat, Communications Earth & Environment, 1, 1, https://doi.org/10.1038/s43247-020-0001-2, 2020.

Kriegler, E., Hall, J. W., Held, H., Dawson, R., and Schellnhuber, H. J.: Imprecise probability assessment of tipping points in the climate system, Proceedings of the National Academy of Sciences of the United States of America, 106, 5041–5046, https://doi.org/10.1073/pnas.0809117106, 2009.

Le Quéré, C., Andrew, R. M., Canadell, J. G., Sitch, S., Ivar Korsbakken, J., Peters, G. P., Manning, A. C., Boden, T. A., Tans, P. P., Houghton, R. A., Keeling, R. F., Alin, S., Andrews, O. D., Anthoni, P., Barbero, L., Bopp, L., Chevallier, F., Chini, L. P., Ciais, P., Currie, K., Delire, C., Doney, S. C., Friedlingstein, P., Gkritzalis, T., Harris, I., Hauck, J., Haverd, V., Hoppema, M., Klein Goldewijk, K., Jain, A. K., Kato, E., Körtzinger, A., Landschützer, P., Lefèvre, N., Lenton, A., Lienert, S., Lombardozzi, D., Melton, J. R., Metzl, N., Millero, F., Monteiro, P. M., Munro, D. R., Nabel, J. E., Nakaoka, S. I., O'Brien, K., Olsen, A., Omar, A. M., Ono, T., Pierrot, D., Poulter, B., Rödenbeck, C., Salisbury, J., Schuster, U., Schwinger, J., Séférian, R., Skjelvan, I., Stocker, B. D., Sutton, A. J., Takahashi, T., Tian, H., Tilbrook, B., Van Der Laan-Luijkx, I. T., Van Der Werf, G. R., Viovy, N., Walker, A. P., Wiltshire, A. J., and Zaehle, S.: Global Carbon Budget 2016, Earth System Science Data, 8, 605–649, https://doi.org/10.5194/essd-8-605-2016, 2016.

Leach, N. J., Jenkins, S., Nicholls, Z., Smith, C. J., Lynch, J., Cain, M., Walsh, T., Wu, B., Tsutsui, J., and Allen, M. R.: FaIRv2.0.0: A generalized impulse response model for climate uncertainty and future scenario exploration, Geoscientific Model Development, 14, 3007–3036, https://doi.org/10.5194/gmd-14-3007-2021, 2021.

Lee, J.-Y., Marotzke, J., Bala, G., Cao, L., Corti, S., Dunne, J., Engelbrecht, F., Fischer, E., Fyfe, J., Jones, C., Maycock, A., Mutemi, J., Ndiaye, O., Panickal, S., and Zhou, T.: Future Global Climate: Scenario-Based Projections and Near-Term Information, in: Climate Change 2021: The Physical Science Basis. Contribution of Working Group I to the Sixth Assessment Report of the Intergovernmental Panel on Climate Change, edited by Masson-Delmotte, V., Zhai, P., Pirani, A., Connors, S., Péan, C., Berger, S., Caud, N., Chen, Y., Goldfarb, L., Gomis, M., Huang, M., Leitzell, K., Lonnoy, E., Matthews, J., Maycock, T., Waterfield, T., Yelekçi, O., Yu, R., and Zhou, B., p. 553–672, Cambridge University Press, Cambridge, United Kingdom and New York, NY, USA, https://doi.org/10.1017/9781009157896.006, 2021.

Lenton, T. M., Held, H., Kriegler, E., Hall, J. W., Lucht, W., Rahmstorf, S., and Schellnhuber, H. J.: Tipping elements in the Earth's climate system, Proceedings of the National Academy of Sciences, 105, 1786–1793, https://doi.org/10.1073/pnas.0705414105, 2008.

Lenton, T. M., Rockström, J., Gaffney, O., Rahmstorf, S., Richardson, K., Steffen, W., and Schellnhuber, H. J.: Climate tipping points — too risky to bet against, Nature, 575, 592–595, 2019.

Liu, W., Xie, S.-P., Liu, Z., and Zhu, J.: Overlooked possibility of a collapsed Atlantic Meridional Overturning Circulation in warming climate, Science Advances, 3, e1601 666, https://doi.org/10.1126/sciadv.1601666, 2017.

Lontzek, T. S., Cai, Y., Judd, K. L., and Lenton, T. M.: Stochastic integrated assessment of climate tipping points indicates the need for strict climate policy, Nature Climate Change, 5, 441–444, https://doi.org/10.1038/nclimate2570, 2015.

Luke, C. M. and Cox, P. M.: Soil carbon and climate change: From the Jenkinson effect to the compost-bomb instability, European Journal of Soil Science, 62, 5–12, https://doi.org/10.1111/j.1365-2389.2010.01312.x, 2011.

McKay, M. D., Beckman, R. J., and Conover, W. J.: A Comparison of Three Methods for Selecting Values of Input Variables in the Analysis of Output from a Computer Code, Technometrics, 21, 239–245, https://doi.org/10.2307/1268522, publisher: [Taylor & Francis, Ltd., American Statistical Association, American Society for Quality], 1979.

Meinshausen, M., Nicholls, Z. R., Lewis, J., Gidden, M. J., Vogel, E., Freund, M., Beyerle, U., Gessner, C., Nauels, A., Bauer, N., Canadell, J. G., Daniel, J. S., John, A., Krummel, P. B., Luderer, G., Meinshausen, N., Montzka, S. A., Rayner, P. J., Reimann, S., Smith, S. J., Van Den Berg, M., Velders, G. J., Vollmer, M. K., and Wang, R. H.: The shared socio-economic pathway (SSP) greenhouse gas concentrations and their extensions to 2500, Geoscientific Model Development, 13, 3571–3605, https://doi.org/10.5194/gmd-13-3571-2020, 2020.

Meinshausen, M., Lewis, J., McGlade, C., Gütschow, J., Nicholls, Z., Burdon, R., Cozzi, L., and Hackmann, B.: Realization of Paris Agreement pledges may limit warming just below 2 °C, Nature, 604, 304–309, https://doi.org/10.1038/s41586-022-04553-z, 2022.

Metropolis, N., Rosenbluth, A. W., Rosenbluth, M. N., Teller, A. H., and Teller, E.: Equation of State Calculations by Fast Computing Machines, The Journal of Chemical Physics, 21, 1087–1092, https://doi.org/10.1063/1.1699114, 1953.

Myhre, G.and Shindell, D., Bréon, F.-M., Collins, W.and Fuglestvedt, J., Huang, J., Koch, D., Lamarque, J.-F., Lee, D.and Mendoza, B., Nakajima, T.and Robock, A., Stephens, G., Takemura, T., and Zhang, H.: Anthropogenic and Natural Radiative Forcing, in: Climate Change 2013: The Physical Science Basis. Contribution of Working Group I to the Fifth Assessment Report of the Intergovernmental Panel on Climate Change, edited by Stocker, T. F., Qin, D., Plattner, G.-K., Tignor, M., Allen, S. K., Boschung, J., Nauels, A., Xia, Y., Bex, V., and Midgley, P. M., chap. 8, pp. 650–740, Cambridge University Press, Cambridge, United Kingdom and New York, NY, USA, https://doi.org/10.1017/CBO9781107415324.018, 2013.

Nicholls, Z. R. J., Meinshausen, M., Lewis, J., Gieseke, R., Dommenget, D., Dorheim, K., Fan, C.-S., Fuglestvedt, J. S., Gasser, T., Golueke, U., Goodwin, P., Hartin, C., Hope, A. P., Kriegler, E., Leach, N. J., Marchegiani, D., McBride, L. A., Quilcaille, Y., Rogelj, J., Salawitch,

R. J., Samset, B. H., Sandstad, M., Shiklomanov, A. N., Skeie, R. B., Smith, C. J., Smith, S., Tanaka, K., Tsutsui, J., and Xie, Z.: Reduced
Complexity Model Intercomparison Project Phase 1: introduction and evaluation of global-mean temperature response, Geoscientific
Model Development, 13, 5175–5190, https://doi.org/10.5194/gmd-13-5175-2020, 2020.

Nobre, C. A., Sampaio, G., Borma, L. S., Castilla-Rubio, J. C., Silva, J. S., and Cardoso, M.: Land-use and climate change risks in the
amazon and the need of a novel sustainable development paradigm, Proceedings of the National Academy of Sciences of the United States
of America, 113, 10 759–10 768, https://doi.org/10.1073/pnas.1605516113, 2016.

Olefeldt, D., Goswami, S., Grosse, G., Hayes, D., Hugelius, G., Kuhry, P., Mcguire, A. D., Romanovsky, V. E., Sannel, A. B., Schuur,
E. A., and Turetsky, M. R.: Circumpolar distribution and carbon storage of thermokarst landscapes, Nature Communications, 7, 1–11,
https://doi.org/10.1038/ncomms13043, 2016.

O'Neill, B. C., Tebaldi, C., Van Vuuren, D. P., Eyring, V., Friedlingstein, P., Hurtt, G., Knutti, R., Kriegler, E., Lamarque, J. F., Lowe,
J., Meehl, G. A., Moss, R., Riahi, K., and Sanderson, B. M.: The Scenario Model Intercomparison Project (ScenarioMIP) for CMIP6,
Geoscientific Model Development, 9, 3461–3482, https://doi.org/10.5194/gmd-9-3461-2016, 2016.

Parry, I., Ritchie, P., and Cox, P.: Evidence of Amazon rainforest dieback in CMIP6 models, EGUsphere, pp. 1–11, http://arxiv.org/abs/2203.
11744, 2022.

Rignot, E., Mouginot, J., Morlighem, M., Seroussi, H., and Scheuchl, B.: Widespread, rapid grounding line retreat of Pine Is-
land, Thwaites, Smith, and Kohler glaciers, West Antarctica, from 1992 to 2011, Geophysical Research Letters, 41, 3502–3509,
https://doi.org/10.1002/2014GL060140, 2014.

Ritchie, P. D., Clarke, J. J., Cox, P. M., and Huntingford, C.: Overshooting tipping point thresholds in a changing climate, Nature, 592,
517–523, https://doi.org/10.1038/s41586-021-03263-2, publisher: Springer US, 2021.

Robinson, A., Calov, R., and Ganopolski, A.: Multistability and critical thresholds of the Greenland ice sheet, Nature Climate Change, 2,
429–432, https://doi.org/10.1038/nclimate1449, 2012.

Schneider von Deimling, T., Grosse, G., Strauss, J., Schirrmeister, L., Morgenstern, A., Schaphoff, S., Meinshausen, M., and Boike, J.:
Observation-based modelling of permafrost carbon fluxes with accounting for deep carbon deposits and thermokarst activity, Biogeo-
sciences, 12, 3469–3488, https://doi.org/10.5194/bg-12-3469-2015, 2015.

Schuur, E. A., McGuire, A. D., Schädel, C., Grosse, G., Harden, J. W., Hayes, D. J., Hugelius, G., Koven, C. D., Kuhry, P., Lawrence,
D. M., Natali, S. M., Olefeldt, D., Romanovsky, V. E., Schaefer, K., Turetsky, M. R., Treat, C. C., and Vonk, J. E.: Climate change and the
permafrost carbon feedback, Nature, 520, 171–179, https://doi.org/10.1038/nature14338, 2015.

Science Panel for the Amazon: Executive Summary, in: Science Panel for the Amazon Amazon Assessment Report 2021, edited by Nobre,
C., Encalada, A., Anderson, E., Roca Alcazar, F., Bustamante, M., Mena, C., Peña-Claros, M., Poveda, G., Rodriguez, J., Saleska, S.,
Trumbore, S., Val, A., Nova, L. V., Abramovay, R., Alencar, A., Alzza, A., Armenteras, D., Artaxo, P., Athayde, S., Barretto Filho,
H., Barlow, J., Berenguer, E., Bortolotto, F., Costa, F., Costa, M., Cuvi, N., Fearnside, P., Ferreira, J., Flores, B., Frieri, S., Gatti, L.,
Guayasamin, J., Hecht, S., Hirota, M., Hoorn, C., Josse, C., Lapola, D., Larrea, C., Larrea-Alcazar, D., Lehm Ardaya, Z., Malhi, Y.,
Marengo, J., Moraes, M., Moutinho, P., Murmis, M., Neves, E., Paez, B., Painter, L., Ramos, A., Rosero-Peña, M., Schmink, M., Sist,
P., Ter Steege, H., Val, P., Van der Voort, H., Varese, M., and Zapata-Ríos, p. 48, United Nations Sustainable Development Solutions
Network, New York, 2021.

Shepherd, A., Gilbert, L., Muir, A. S., Konrad, H., McMillan, M., Slater, T., Briggs, K. H., Sundal, A. V., Hogg, A. E., and Engdahl, M. E.:
Trends in Antarctic Ice Sheet Elevation and Mass, Geophysical Research Letters, 46, 8174–8183, https://doi.org/10.1029/2019GL082182,
2019.

Smith, C. J.: Effective Radiative Forcing Time Series from the Shared Socioeconomic Pathways, https://doi.org/10.5281/zenodo.3973015, 2020.

Steffen, W., Rockström, J., Richardson, K., Lenton, T. M., Folke, C., Liverman, D., Summerhayes, C. P., Barnosky, A. D., Cornell, S. E., Crucifix, M., Donges, J. F., Fetzer, I., Lade, S. J., Scheffer, M., Winkelmann, R., and Schellnhuber, H. J.: Trajectories of the Earth System in the Anthropocene, https://doi.org/10.1073/pnas.1810141115, 2018.

Turetsky, M. R., Abbott, B. W., Jones, M. C., Anthony, K. W., Olefeldt, D., Schuur, E. A. G., Koven, C., McGuire, A. D., Grosse, G., Kuhry, P., Hugelius, G., Lawrence, D. M., Gibson, C., and Sannel, A. B. K.: Permafrost collapse is accelerating carbon release, Nature, pp. 32–34, https://www.nature.com/articles/d41586-019-01313-4, 2019.

Turetsky, M. R., Abbott, B. W., Jones, M. C., Anthony, K. W., Olefeldt, D., Schuur, E. A., Grosse, G., Kuhry, P., Hugelius, G., Koven, C., Lawrence, D. M., Gibson, C., Sannel, A. B. K., and McGuire, A. D.: Carbon release through abrupt permafrost thaw, Nature Geoscience, 13, 138–143, https://doi.org/10.1038/s41561-019-0526-0, 2020.

United Nations Environment Programme: Emissions Gap Report 2022: The Closing Window — Climate crisis calls for rapid transformation of societies, https://www.unep.org/resources/emissions-gap-report-2022, 2022.

Van Breedam, J., Goelzer, H., and Huybrechts, P.: Semi-equilibrated global sea-level change projections for the next 10 000 years, Earth System Dynamics, 11, 953–976, https://doi.org/10.5194/esd-11-953-2020, 2020.

Van Marle, M. J., Kloster, S., Magi, B. I., Marlon, J. R., Daniau, A. L., Field, R. D., Arneth, A., Forrest, M., Hantson, S., Kehrwald, N. M., Knorr, W., Lasslop, G., Li, F., Mangeon, S., Yue, C., Kaiser, J. W., and Van Der Werf, G. R.: Historic global biomass burning emissions for CMIP6 (BB4CMIP) based on merging satellite observations with proxies and fire models (1750-2015), Geoscientific Model Development, 10, 3329–3357, https://doi.org/10.5194/gmd-10-3329-2017, 2017.

Wang, S., Foster, A., Lenz, E. A., Kessler, J. D., Stroeve, J. C., Anderson, L. O., Turetsky, M., Betts, R., Zou, S., Liu, W., Boos, W. R., and Hausfather, Z.: Mechanisms and Impacts of Earth System Tipping Elements, Reviews of Geophysics, 61, https://doi.org/10.1029/2021RG000757, 2023.

Wunderling, N., Donges, J. F., Kurths, J., and Winkelmann, R.: Interacting tipping elements increase risk of climate domino effects under global warming, Earth System Dynamics, 12, 601–619, https://doi.org/10.5194/esd-12-601-2021, 2021.